Improved Constraints on Cosmology and Foregrounds from BICEP2 and Keck Array Cosmic Microwave Background Data with Inclusion of 95 GHz Band

Improved Constraints on Cosmology and Foregrounds from BICEP2 and Keck Array Cosmic Microwave Background Data with Inclusion of 95 GHz Band

P. A. R. Ade,[1] Z. Ahmed,[2,3] R. W. Aikin,[4] K. D. Alexander,[5] D. Barkats,[5] S. J. Benton,[6] C. A. Bischoff,[5] J. J. Bock,[4,7] R. Bowens-Rubin,[5] J. A. Brevik,[4] I. Buder,[5] E. Bullock,[8] V. Buza,[5,9] J. Connors,[5] B. P. Crill,[7] L. Duband,[10] C. Dvorkin,[9] J. P. Filippini,[4,11] S. Fliescher,[12] J. Grayson,[3] M. Halpern,[13] S. Harrison,[5] G. C. Hilton,[14] H. Hui,[4] K. D. Irwin,[3,2,14] K. S. Karkare,[5] E. Karpel,[3] J. P. Kaufman,[15] B. G. Keating,[15] S. Kefeli,[4] S. A. Kernasovskiy,[3] J. M. Kovac,[5,9,*] C. L. Kuo,[3,2] E. M. Leitch,[16] M. Lueker,[4] K. G. Megerian,[7] C. B. Netterfield,[6,17] H. T. Nguyen,[7] R. O'Brient,[4,7] R. W. Ogburn IV,[3,2] A. Orlando,[4,15] C. Pryke,[12,8,†] S. Richter,[5] R. Schwarz,[12] C. D. Sheehy,[12,16] Z. K. Staniszewski,[4,7] B. Steinbach,[4] R. V. Sudiwala,[1] G. P. Teply,[4,15] K. L. Thompson,[3,2] J. E. Tolan,[3] C. Tucker,[1] A. D. Turner,[7] A. G. Vieregg,[5,18,16] A. C. Weber,[7] D. V. Wiebe,[13] J. Willmert,[12] C. L. Wong,[5,9] W. L. K. Wu,[3] and K. W. Yoon[3,2]

(Keck Array and BICEP2 Collaborations)

[1]*School of Physics and Astronomy, Cardiff University, Cardiff, CF24 3AA, United Kingdom*
[2]*Kavli Institute for Particle Astrophysics and Cosmology, SLAC National Accelerator Laboratory, 2575 Sand Hill Road, Menlo Park, California 94025, USA*
[3]*Department of Physics, Stanford University, Stanford, California 94305, USA*
[4]*Department of Physics, California Institute of Technology, Pasadena, California 91125, USA*
[5]*Harvard-Smithsonian Center for Astrophysics, 60 Garden Street MS 42, Cambridge, Massachusetts 02138, USA*
[6]*Department of Physics, University of Toronto, Toronto, Ontario, M5S 1A7, Canada*
[7]*Jet Propulsion Laboratory, Pasadena, California 91109, USA*
[8]*Minnesota Institute for Astrophysics, University of Minnesota, Minneapolis, Minnesota 55455, USA*
[9]*Department of Physics, Harvard University, Cambridge, Massachusetts 02138, USA*
[10]*Service des Basses Températures, Commissariat à l'Energie Atomique, 38054 Grenoble, France*
[11]*Department of Physics, University of Illinois at Urbana-Champaign, Urbana, Illinois 61801, USA*
[12]*School of Physics and Astronomy, University of Minnesota, Minneapolis, Minnesota 55455, USA*
[13]*Department of Physics and Astronomy, University of British Columbia, Vancouver, British Columbia, V6T 1Z1, Canada*
[14]*National Institute of Standards and Technology, Boulder, Colorado 80305, USA*
[15]*Department of Physics, University of California at San Diego, La Jolla, California 92093, USA*
[16]*Kavli Institute for Cosmological Physics, University of Chicago, Chicago, Illinois 60637, USA*
[17]*Canadian Institute for Advanced Research, Toronto, Ontario M5G 1Z8, Canada*
[18]*Department of Physics, Enrico Fermi Institute, University of Chicago, Chicago, Illinois 60637, USA*

(Received 2 November 2015; published 20 January 2016)

We present results from an analysis of all data taken by the BICEP2 and Keck Array cosmic microwave background (CMB) polarization experiments up to and including the 2014 observing season. This includes the first Keck Array observations at 95 GHz. The maps reach a depth of 50 nK deg in Stokes Q and U in the 150 GHz band and 127 nK deg in the 95 GHz band. We take auto- and cross-spectra between these maps and publicly available maps from WMAP and Planck at frequencies from 23 to 353 GHz. An excess over lensed ΛCDM is detected at modest significance in the 95×150 BB spectrum, and is consistent with the dust contribution expected from our previous work. No significant evidence for synchrotron emission is found in spectra such as 23×95, or for correlation between the dust and synchrotron sky patterns in spectra such as 23×353. We take the likelihood of all the spectra for a multicomponent model including lensed ΛCDM, dust, synchrotron, and a possible contribution from inflationary gravitational waves (as parametrized by the tensor-to-scalar ratio r) using priors on the frequency spectral behaviors of dust and synchrotron emission from previous analyses of WMAP and Planck data in other regions of the sky. This analysis yields an upper limit $r_{0.05} < 0.09$ at 95% confidence, which is robust to variations explored in analysis and priors. Combining these B-mode results with the (more model-dependent) constraints from Planck analysis of CMB temperature plus baryon acoustic oscillations and other data yields a combined limit $r_{0.05} < 0.07$ at 95% confidence. These are the strongest constraints to date on inflationary gravitational waves.

DOI: 10.1103/PhysRevLett.116.031302

Introduction.—Measurements of the cosmic microwave background (CMB) [1] are one of the observational pillars of the standard cosmological model (ΛCDM) and constrain its parameters to high precision (see most recently Ref. [2]). This model extrapolates the Universe back to very high temperatures ($\gg 10^{12}$ K) and early times ($\ll 1$ s). Observations indicate that conditions at these early times are described by an almost uniform plasma with a nearly scale invariant spectrum of adiabatic density perturbations. However, ΛCDM itself offers no explanation for how these conditions occurred. The theory of inflation is an extension to the standard model, which postulates a phase of exponential expansion at a still earlier epoch ($\sim 10^{-35}$ s) that precedes ΛCDM and produces the required initial conditions (see Ref. [3] for a recent review and citations to the original literature).

There is widespread support for the claim that existing observations already indicate that some version of inflation probably did occur, but there are also skeptics [4,5]. As well as the specific form of the initial density perturbations, there is an additional relic which inflation predicts, and which one can attempt to detect. Inflation launches tensor mode perturbations into the fabric of space-time, which will propagate unimpeded as inflationary gravitational waves (IGWs) to the present day. Their amplitude is diminished with the expansion of the Universe, and detection at the present epoch is not feasible with current technology. The most promising potential method of detection is to look for their signature written into the pattern of the CMB at last scattering, 380 000 years after the Universe entered the realm of fully known physics. Inflationary theories generically predict that IGWs exist, but many specific models have been proposed producing a wide range of amplitudes—with some being unobservably small [3]. The size of the IGW signal is conventionally expressed as the initial ratio of the tensor and scalar perturbation amplitudes r.

In the ΛCDM standard model the CMB is polarized by Thomson scattering of Doppler induced quadrupoles in the local radiation field at last scattering. This naturally produces a polarization pattern with direction parallel or perpendicular to the gradient of its intensity—this is curl-free, or E-mode polarization, and was first detected in Ref. [6]. Because of small gravitational deflections of the CMB photons in flight by intervening large scale structure, the initial purity of the E-mode pattern is disturbed and a small lensing B mode is produced at subdegree angular scales [7,8].

IGWs are intrinsically quadrupolar distortions of the metric and produce both E- and B-mode polarization depending on their orientation with respect to our last scattering surface. However, due to the large ΛCDM E-mode signal, the most promising place to search for an IGW signal is in B modes. Furthermore, since the IGW B modes have a much redder spectrum than the lensing B modes, the best place to look is at angular scales larger than a few degrees (multipoles $\ell < 100$). Limits on IGW from nonpolarized CMB observations are now fully saturated at cosmic variance limits [2], and it is generally agreed that the best (only) way to make further progress is through improved measurements of CMB B modes.

The BICEP and Keck Array telescopes are small aperture polarimeters specifically designed to search for an IGW signal at the recombination bump ($\ell \approx 80$). BICEP1 operated from 2006 to 2008 and set a limit $r_{0.05} < 0.70$ at 95% confidence [9]. BICEP2 operated from 2010 to 2012 at 150 GHz and in Ref. [10] reported a detection of a substantial excess over the lensed-ΛCDM expectation in the multipole range $30 < \ell < 150$. Additional measurements at 150 GHz taken by the Keck Array during 2012 and 2013 confirmed this excess [11]. However, new data from the Planck space mission provided evidence that emission from galactic dust grains could be more polarized at high galactic latitudes than anticipated [12,13], a possibility emphasized in Refs. [14,15]. Analysis of the combined BICEP2 and Keck Array 150 GHz data in combination with data from Planck (principally at 353 GHz) showed that a substantial part of the 150 GHz excess is due to polarized emission from galactic dust grains, and that once this is accounted for, the result becomes $r_{0.05} < 0.12$ at 95% confidence [16].

BICEP2 was a simple 26 cm aperture all-cold refractor, and Keck Array is basically five copies of this on a single telescope mount [11,17]. Both are sited at the South Pole in Antarctica, taking advantage of the dry atmosphere and stable observing conditions. In addition to the all-cold optics these telescopes have two features which aid greatly in the suppression and characterization of instrumental systematics: (i) they are equipped with comoving absorptive forebaffles resulting in extremely low far side-lobe response, and (ii) the entire instrument can be rotated about the line of sight allowing modulation of polarized signal.

Keck Array was designed at the outset to observe in multiple frequency bands—the 2012 and 2013 observations were all taken at 150 GHz because detectors for other bands were not yet ready. Before the 2014 season two of the five receivers of Keck Array were refitted for operation in a band centered on 95 GHz (the other three receivers remaining unchanged at 150 GHz). In this Letter we fold in this new data and perform a multicomponent, multispectral likelihood analysis similar to our previous analysis [16].

This Letter builds on the initial BICEP2 results Letter [10] (hereafter BK-I), the Keck 2012 + 2013 results paper [11] (BK-V), and the BICEP2/Keck/Planck analysis Letter [16] (BKP).

Instrument and observations.—The Keck Array instrument is described in Sec. 2 of BK-V [11] (see also the BICEP2 Instrument paper [17] for further details). Before the 2014 observing season, two of the receivers of Keck Array were removed, the lenses and filters were replaced with versions optimized for a band centered at 95 GHz,

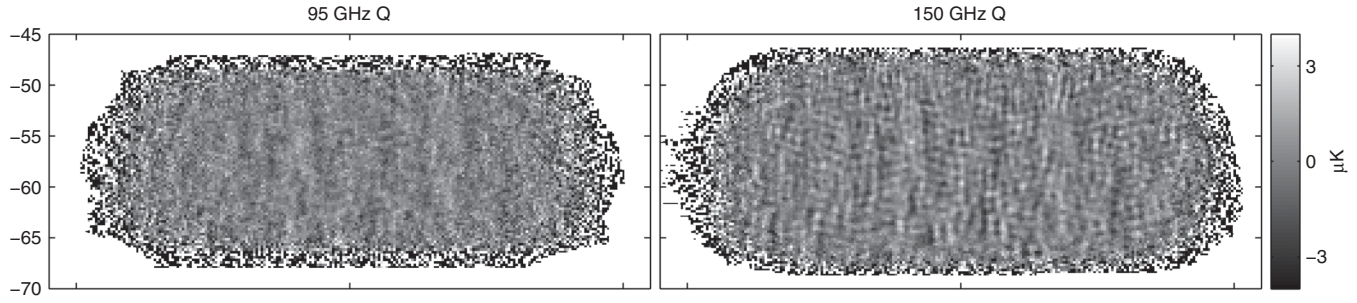

FIG. 1. Deep Q maps at 95 and 150 GHz using all BICEP2/Keck data through the end of the 2014 observing season—we refer to these maps as BK14. Noise levels are 127 nK deg (left) and 50 nK deg (right). Both maps show a high signal-to-noise pattern dominated by E-mode polarization; the 95 GHz maps appear smoother because of the larger beam size.

and the focal planes were replaced with units loaded with appropriately scaled versions of our antenna-coupled detectors [18]. Because the physical size of these antennas is larger, each of the four tiles contains only a 6×6 array (rather than 8×8 at 150 GHz). With two focal planes at 95 GHz, this gives 288 total detector pairs (576 total detectors).

During the 2014 austral winter season the array was operated exactly as for the previous seasons. A ∼1% region of sky centered at RA 0h, Dec. −57.5° was observed from March until November over ≈4600 50-min "scan sets." The efficiency and yield was similar to previous seasons. See Sec. 4 of BK-V [11] for further details of the observing strategy and data selection.

BICEP2/Keck maps.—The processing from time stream to maps is identical to that described in Secs. III and IV of BK-I [10] and summarized in Sec. 5 of BK-V [11]. Relative gain calibration is applied between the two halves of each pair and the difference is taken. Filtering is then applied to remove residual atmospheric noise and any ground-fixed (scan-synchronous) pickup. The data are then binned into simple map pixels and, with knowledge of the polarization sensitivity directions, maps of Stokes parameters Q and U are formed. "Deprojection" is also performed to remove leakage of temperature to polarization due to beam systematics, and this results in an additional filtering of signal.

Figure 1 shows the 95 and 150 GHz Q maps combining data from BICEP2 (2010–2012) and Keck Array (2012–2014)—we refer to these as the BK14 maps meaning that they contain all data up to and including that taken during the 2014 observing season. The 150 GHz maps add 3 more receiver years to the previous 13 in the BK13-based analysis of BKP [16], and modestly improves the Q/U sensitivity from 57 to 50 nK deg (3.0 μK arcmin) over an

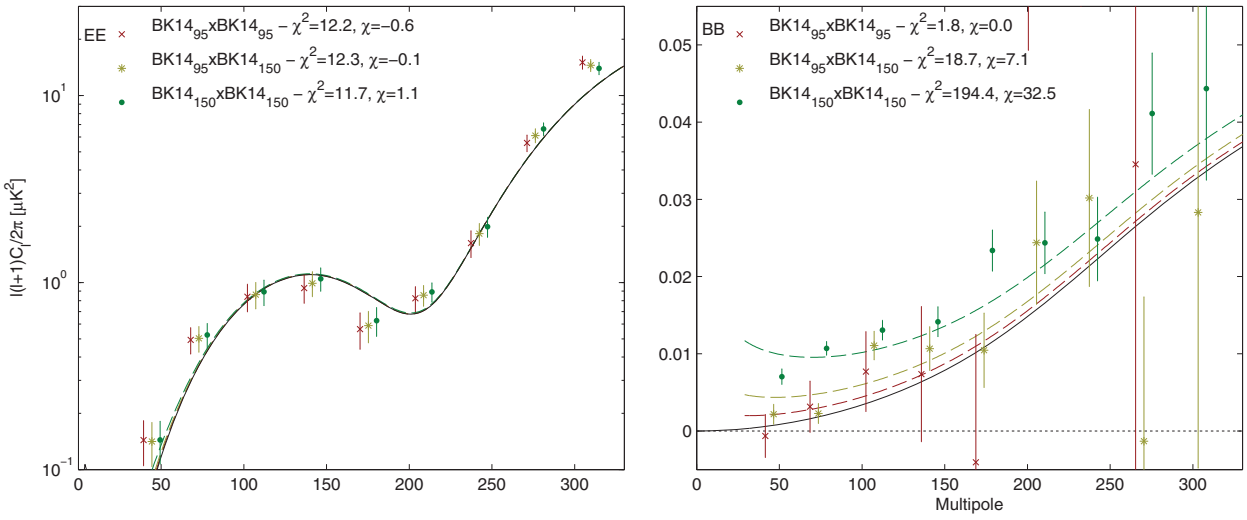

FIG. 2. *EE* and *BB* auto- and cross-spectra between 95 and 150 GHz using all BICEP2/Keck data up to and including that taken during the 2014 observing season—we refer to these spectra as BK14. (For clarity the sets of points are offset horizontally.) The solid black curves show the lensed-ΛCDM theory spectra. The error bars are the standard deviations of the lensed-ΛCDM + noise simulations and hence contain no sample variance on any additional signal component. The χ^2 and χ (sum of deviations) against lensed ΛCDM for the lowest five band powers are given, and can be compared to their expectation value/standard deviation of 5/3.1 and 0/2.2, respectively The dashed lines show a lensed-ΛCDM+dust model derived from our previous BKP [16] analysis.

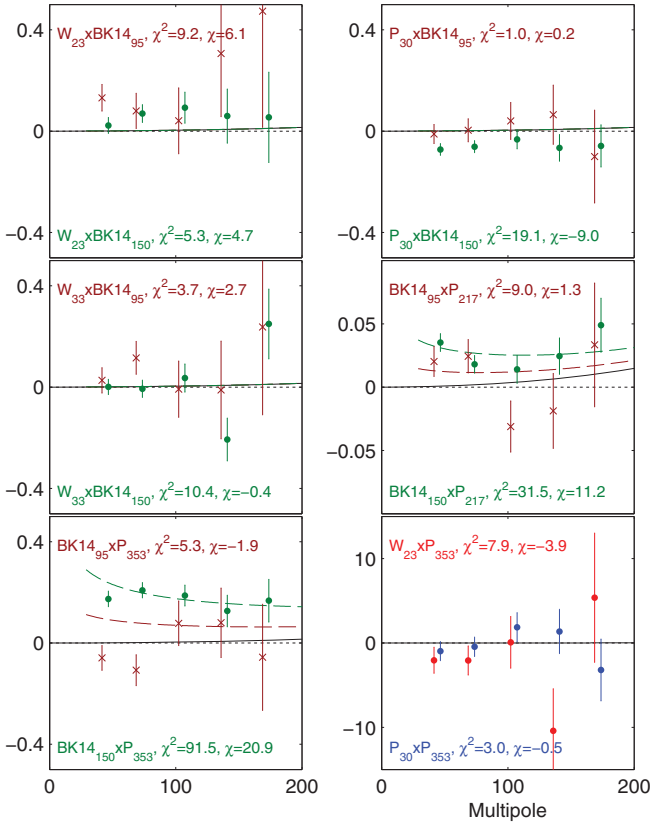

FIG. 3. Selected *BB* cross-spectra between the BK14 maps at 95 (red) and 150 GHz (green) and the external maps of WMAP and Planck. The quantity plotted is $\ell(\ell+1)C_l/2\pi$ (μK^2), and the error bars are the standard deviations of the lensed-ΛCDM + noise simulations. The solid black curves show the lensed-ΛCDM theory spectrum and the χ^2 and χ versus this model are shown. $W_{23} \times BK14_{95}$ and $W_{23} \times BK14_{150}$ are both mildly elevated showing weak evidence for synchrotron, but $P_{30} \times BK14_{150}$ has stronger nominal anticorrelation. We see modest evidence for detection of dust emission in $BK14_{150} \times P_{217}$ and strong evidence in $BK14_{150} \times P_{353}$. The dashed lines show a lensed-ΛCDM+dust model derived from our previous BKP [16] analysis.

effective area of 395 square degrees. These are the deepest maps of CMB polarization published to date. The 95 GHz maps contain only 2 receiver years of data and the Q/U sensitivity is 127 nK deg (7.6 μK arcmin) over an effective area of 375 square degrees. [The survey weight is thus 310000 (47000) μK^{-2} at 150 (95) GHz.] The 95 GHz beam is wider (43 versus 30 arcmin FWHM), and we see the effect of the additional beam smoothing. However, the degree scale structure is clearly nearly identical at both frequencies. While there is a dust component hidden in the 150 GHz maps, it is highly subdominant to the ΛCDM *E*-mode signal. See Appendix A in the Supplemental Material [19] for the full set of $T/Q/U$ signal and noise maps.

External maps.—We use the public release 2 "full mission" maps available from the Planck Legacy Archive [22,23], noting that these are nearly identical to those used in BKP [16]. For this analysis we also add the WMAP9 23 GHz (*K*-band) and 33 GHz (*Ka*-band) maps [24,25].

For each of these external maps we deconvolve the native instrument beam, reconvolve the Keck 150 GHz beam, and then process the result through an "observing" matrix to produce a map with the same filtering of spatial modes as the 150 GHz map. See Sec. II A of BKP [16] for further details of this process. For Planck we use the FFP8 simulations [26], and for WMAP we use simple inhomogeneous white noise simulations derived from the provided variance maps.

Power spectra.—We convert the maps to power spectra using the methods described in Sec. VI of BK-I [10] including the matrix-based purification operation to prevent *E* to *B* mixing. We generate separate purification matrices to match the filtering of the 95 and 150 GHz maps.

We first subject the new 95 GHz data to our usual suite of "jackknife" internal consistency checks. The results are given in Appendix B of the Supplemental Material [19] and show empirically that the data are free of systematic contamination at a level greater than the noise. In addition, in Appendix C of the Supplemental Material [19] we investigate the stability of the previous 150 GHz spectrum when adding the new 2014 data—there is no indication of problems.

We now proceed to comparing the spectra and cross-spectra of our 95 and 150 GHz maps—Fig. 2 shows the results. We use a common apodization mask as the geometric mean of the two (smoothed) inverse variance maps. The *EE* spectra agree to within much better than the nominal error bar size because the uncertainty is dominated by sample variance and we are observing the same piece of sky. To make a rough estimate of the significance of deviation from lensed ΛCDM, we calculate χ^2 and χ (sum of normalized deviations) as shown in the plot. We see strong evidence for excess *BB* power in $BK14_{150} \times BK14_{150}$ and moderate evidence in $BK14_{95} \times BK14_{150}$. Dashed lines for the lensed-ΛCDM + dust model derived in BKP [16] are overplotted and appear to be consistent with the new data.

Figure 3 shows selected *BB* cross-spectra between the BK14 95 and 150 GHz maps and the Planck (P) and WMAP (W) bands. There is no strong evidence for detection of synchrotron emission—$W_{23} \times BK14_{95}$ and $W_{23} \times BK14_{150}$ are both mildly elevated but $P_{30} \times BK14_{150}$ has stronger nominal anticorrelation (as noted in the BKP Letter [16]). $W_{33} \times BK14_{95}$ and $W_{33} \times BK14_{150}$ are both consistent with null. The only strong detections of excess signal are in $BK14_{150} \times P_{353}$ and, at lower significance, $BK14_{150} \times P_{217}$. See Appendix D of the Supplemental Material [19] for the full set of auto- and cross-spectra.

Likelihood analysis.—We next proceed to a multi-component, multispectral likelihood analysis, which is an expanded version of that described in Sec. III of the BKP Letter [16]. We compute the likelihood of the data for

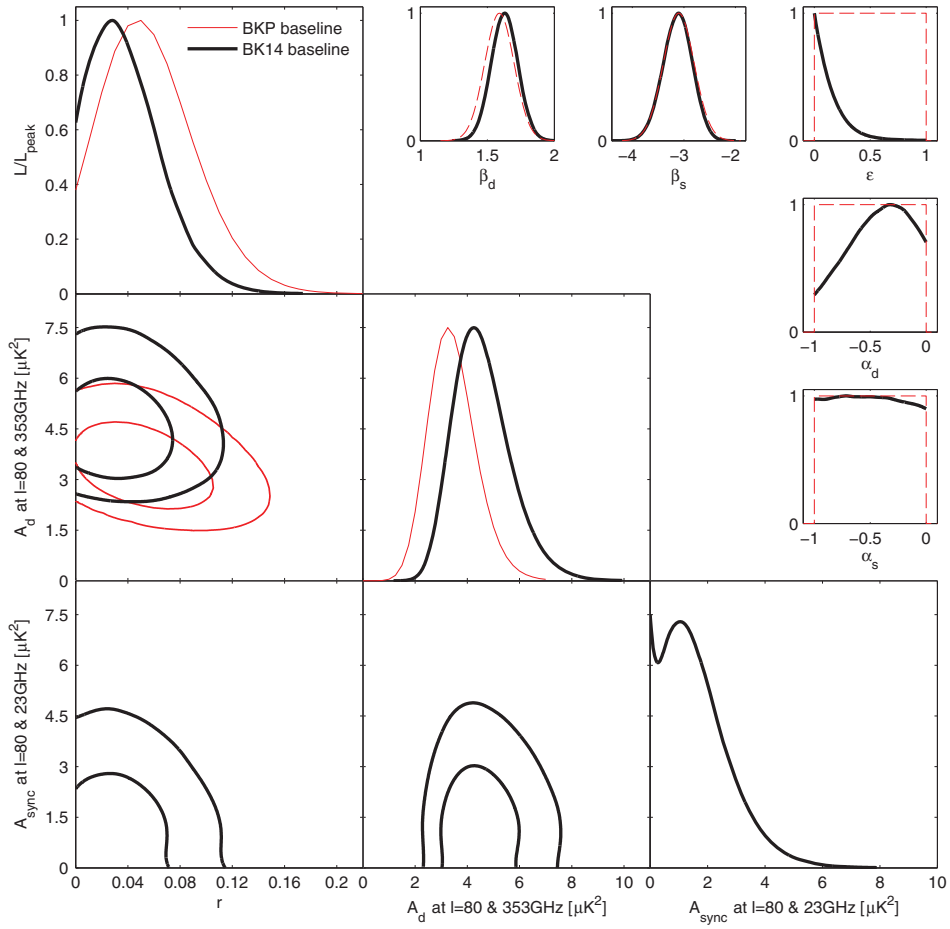

FIG. 4. Results of a multicomponent multispectral likelihood analysis of BICEP2/Keck + external data. The red faint curves are the primary result from the previous BKP Letter [16] (the black curves from Fig. 6 of that Letter). The bold black curves are the new baseline BK14 results. Differences between these analyses include adding synchrotron to the model, including additional external frequency bands from WMAP and Planck, and adding Keck Array data taken during the 2014 observing season at 95 and 150 GHz. We see that the peak position of the tensor/scalar ratio curve r shifts down slightly and the upper limit tightens to $r_{0.05} < 0.09$ at 95% confidence. The parameters A_d and $A_{\rm sync}$ are the amplitudes of the dust and synchrotron B-mode power spectra, where β and α are the respective frequency and spatial spectral indices. The correlation coefficient between the dust and synchrotron patterns is ϵ. In the β, α, and ϵ panels the dashed red lines show the priors placed on these parameters (either Gaussian or uniform).

any given proposed model using an extended version of the Hamimeche-Lewis approximation [27] and the full covariance matrix of the auto- and cross-spectral band powers as derived from simulations (setting to zero terms whose expectation value is zero).

In this analysis we primarily use a lensed-ΛCDM + dust + synchrotron + r model and explore the parameter space using COSMOMC [28]. In this Letter the "baseline" analysis is defined as follows.

(1) Use the BK14 maps as shown in Fig. 1 (all BICEP2/Keck data up to and including that taken during the 2014 observing season).

(2) Use all the polarized bands of Planck (30–353 GHz) plus the 23 and 33 GHz bands of WMAP.

(3) Use all possible BB auto- and cross-spectra between these maps. This includes all the spectra shown in Figs. 2 and 3—the complete set is shown in Appendix D of the Supplemental Material [19]. Spectra with no detection can, of course, still have constraining power; for instance, nondetection in $P_{30} \times P_{353}$ disfavors sync-dust correlation.

(4) Use nine band powers spanning the range $20 < \ell < 330$.

(5) Include dust with amplitude $A_{d,353}$ evaluated at 353 GHz and $\ell = 80$. As in the BKP [16] analysis, the frequency spectral behavior is taken as a simple modified blackbody spectrum with $T_d = 19.6$ K and $\beta_d = 1.59 \pm 0.11$, using a Gaussian prior with the given 1σ width. Analyzing polarized emission at intermediate galactic latitudes, Fig. 11 of Ref. [29] shows that this model is accurate in the mean to within a few percent over the frequency range 100–353 GHz, while the patch-to-patch fluctuation is noise dominated. The spatial power spectrum is taken as a simple power law $\mathcal{D}_\ell \propto \ell^{\alpha_d}$ marginalizing over the range $-1 < \alpha_d < 0$, where $\mathcal{D}_\ell \equiv \ell(\ell+1)C_l/2\pi$.

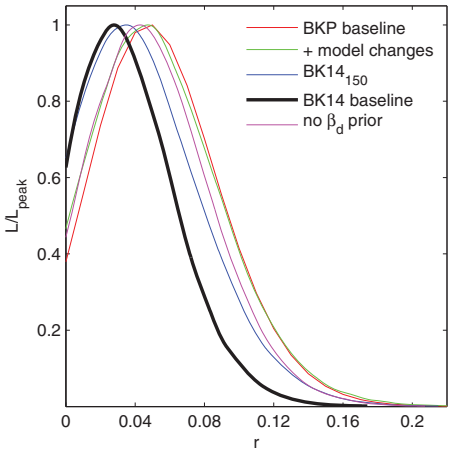

FIG. 5. Likelihood results on r for several intermediate steps between the BKP [16] (previous) and BK14 (current) analyses. See text for details.

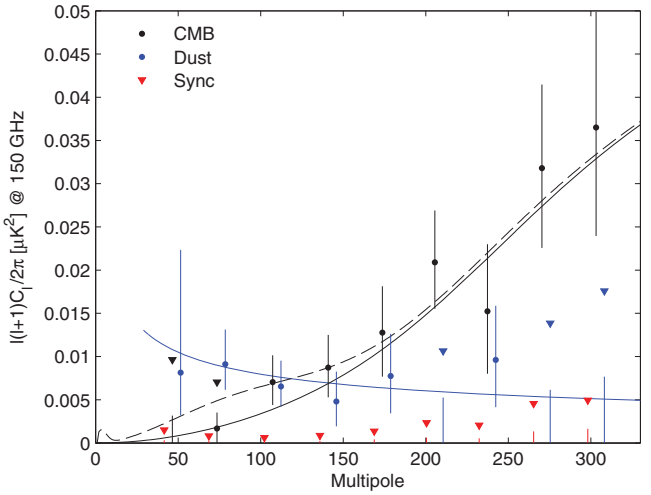

FIG. 6. Spectral decomposition of the BB data into synchrotron (red), CMB (black), and dust (blue) components. The decomposition is calculated independently in each band power, marginalizing over β_d, β_s, and ϵ with the same priors as the baseline analysis. Error bars denote 68% credible intervals, with the point marking the most probable value. If the 68% interval includes zero, we also indicate the 95% upper limit with a downward triangle. (For clarity, the sets of points are offset horizontally.) The solid black line shows lensed ΛCDM with the dashed line adding on top an $r_{0.05} = 0.05$ tensor contribution. The blue curve shows a dust model consistent with the baseline analysis ($A_{d,353} = 4.3\ \mu\mathrm{K}^2$, $\beta_d = 1.6$, $\alpha_d = -0.4$).

(6) Include synchrotron with amplitude $A_{\mathrm{sync},23}$ evaluated at 23 GHz (the lowest WMAP band) and $\ell = 80$, assuming a simple power law for the frequency spectral behavior $A_{\mathrm{sync}} \propto \nu^{\beta_s}$ with a Gaussian prior $\beta_s = -3.1 \pm 0.3$ [30]. The spatial power spectrum is taken as a simple power law $\mathcal{D}_\ell \propto \ell^{\alpha_s}$ marginalizing over the range $-1 < \alpha_s < 0$.

(7) Allow sync-dust correlation and marginalize over the correlation parameter $0 < \epsilon < 1$.

(8) Quote the tensor/scalar power ratio r at a pivot scale of 0.05 Mpc^{-1} and fix the tensor spectral index $n_t = 0$.

See Appendix E1 of the Supplemental Material [19] for a more detailed explanation of these choices.

Results of this baseline analysis are shown in Fig. 4 and yield the following statistics: $r_{0.05} = 0.028^{+0.026}_{-0.025}$, $r_{0.05} < 0.090$ at 95% confidence, $A_{d,353} = 4.3^{+1.2}_{-1.0}\ \mu\mathrm{K}^2$, and $A_{\mathrm{sync},23} < 3.8\ \mu\mathrm{K}^2$ at 95% confidence. For r the zero-to-peak likelihood ratio is 0.63. Taking $\frac{1}{2}[1 - f(-2\log L_0/L_{\mathrm{peak}})]$, where f is the χ^2 CDF (for one degree of freedom), we estimate that the probability to get a likelihood ratio smaller than this is 18% if, in fact, $r = 0$. Running the analysis on the lensed-ΛCDM + dust + noise simulations produces a similar number. The zero-to-peak likelihood ratio for A_d indicates that the detection of dust is now $> 8\sigma$.

Results for the additional parameters are shown in the upper right-hand part of Fig. 4. The dust frequency spectral parameter β_d pulls weakly against the prior to higher values. The synchrotron frequency spectral parameter β_s just reflects the prior (as expected since synchrotron is not strongly detected). The data have a mild preference for values of α_d close to the −0.42 found in Ref. [13], while α_s is unconstrained. The data disfavor strong sync-dust correlation (due to the nondetection of signal in spectra like $\mathrm{W}_{23} \times \mathrm{P}_{353}$; see Fig 3). As A_{sync} approaches zero, ϵ becomes unconstrained, leading to an increase in the available parameter volume, and the "flare" in the A_{sync} constraints.

The maximum likelihood model (including priors) has parameters $r_{0.05} = 0.026$, $A_{d,353} = 4.1\,\mu\mathrm{K}^2$, $A_{\mathrm{sync},23} = 1.4\,\mu\mathrm{K}^2$, $\beta_d = 1.6$, $\beta_s = -3.1$, $\alpha_d = -0.19$, $\alpha_s = -0.56$, and $\epsilon = 0.00$. This model appears to be an acceptable fit to the data; see Appendix D of the Supplemental Material [19] for further details.

In Fig. 4 we see that, as compared to the primary BKP [16] analysis, the peak position of the likelihood curve for r has shifted down slightly. In Fig. 5 we investigate why. Although we have made extensive changes to the model, these make only a small difference (see Appendix E1 of the Supplemental Material [19] for details of these changes). The change from the BK13$_{150}$ to the BK14$_{150}$ maps causes some of the downward shift in the peak position. This may seem surprising given that only a relatively small amount of additional data has been added (∼20%). However, Appendix C in the Supplemental Material [19] shows that the shifts in the band power values are not unlikely and we should therefore accept the shift in the r constraint as simply due to noise fluctuation. Adding in the BK14$_{95}$ data produces an additional downward shift in the peak position, and also significantly narrows the likelihood curve.

Figure 5 shows one additional variation. It turns out that the tight prior on β_d from Planck analysis of other regions of the sky is becoming unnecessary. Removing the prior the peak position of the likelihood on r shifts up slightly and broadens so that $r_{0.05} = 0.043^{+0.033}_{-0.031}$ and $r_{0.05} < 0.11$ (95%), while the likelihood curve for β_d is close to

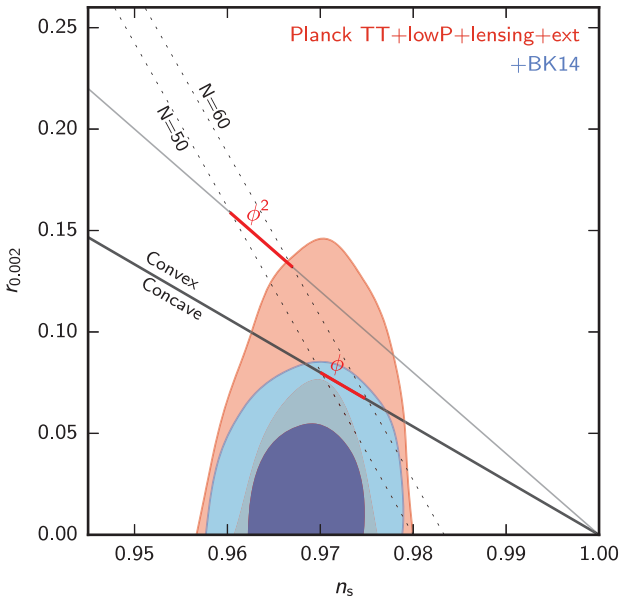

FIG. 7. Constraints in the r vs n_s plane when using Planck plus additional data, and when also adding BICEP2/Keck data through the end of the 2014 season including new 95 GHz maps—the constraint on r tightens from $r_{0.05} < 0.12$ to $r_{0.05} < 0.07$. This figure is adapted from Fig. 21 of Ref. [2]; see there for further details.

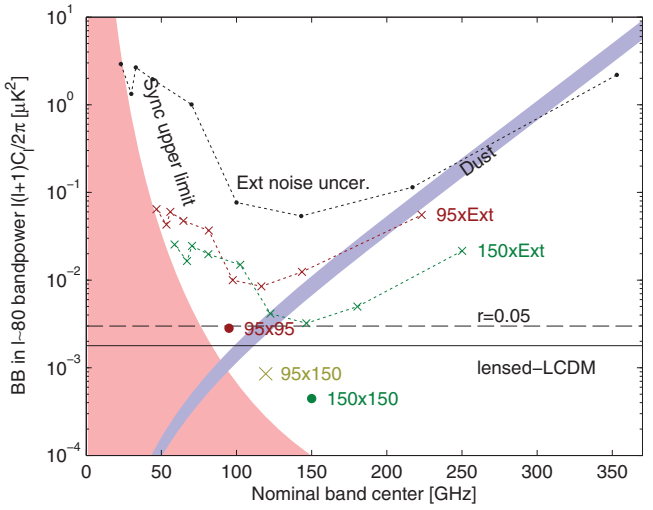

FIG. 8. Expectation values and noise uncertainties for the $\ell \sim 80$ BB band power in the BICEP2/Keck field. The solid and dashed black lines show the expected signal power of lensed ΛCDM and $r_{0.05} = 0.05$. Since CMB units are used, the levels corresponding to these are flat with frequency. The blue band shows a dust model consistent with the baseline analysis ($A_{d,353} = 4.3^{+1.2}_{-1.0}$ μK^2, $\beta_d = 1.6$), while the pink shaded region shows the allowed region for synchrotron ($A_{\mathrm{sync},23} < 3.8$ μK^2, $\beta_s = -3.1$). The BICEP2/Keck noise uncertainties are shown as large colored symbols, and the noise uncertainties of the WMAP/Planck single-frequency spectra evaluated in the BICEP2/Keck field are shown in black. The red (green) crosses show the noise uncertainty of the cross-spectra taken between 95 (150) GHz and, from left to right, 23, 30, 33, 44, 70, 100, 143, 217, and 353 GHz, and are plotted at horizontal positions such that they can be compared vertically with the dust and sync curves.

Gaussian in shape with mean/σ of 1.82/0.26. In Appendix E2 we investigate a variety of other variations from the baseline analysis and in Appendix E3 we perform some validation tests of the likelihood using simulations (the Supplemental Material [19]).

For the purposes of presentation we also run a likelihood analysis to find the CMB and foreground contributions on a band power by band power basis. The baseline analysis is a single fit to all 9 band powers across 66 spectra with 8 parameters. Instead, we now perform 9 separate fits—one for each band power—across the 66 spectra, with 6 parameters in each fit. These 6 parameters are the amplitudes of CMB, dust, and synchrotron plus β_d, β_s, and ϵ with identical priors to the baseline analysis. The results are shown in Fig. 6—the resulting CMB band powers are consistent with lensed ΛCDM while the dust band powers are consistent with the level of dust found in the baseline analysis. Synchrotron is tightly limited in all the band powers.

Conclusions.—As shown above, the BK14 data in combination with external maps produce B-mode-based constraints on the tensor-to-scalar ratio r which place an upper limit $r_{0.05} < 0.09$ at 95% confidence. The analysis of Planck full mission TT data in conjunction with external data produces the constraint $r_{0.002} < 0.11$ ($r_{0.05} < 0.12$) at 95% confidence ["Planck TT + lowP + lensing + ext" in Eq. (39b) of Ref. [2]], and is saturated at the cosmic variance limit. The BK14 result constitutes the first B-mode constraints that clearly surpass those from temperature anisotropies. In Fig. 7 we reproduce the results of Ref. [2] in the r versus n_s plane, and show the effect of adding in our BK14 B-mode data. The allowed region tightens and the joint result is $r_{0.05} < 0.07$ (95%), although as emphasized in Ref. [2], the TT derived constraints on r are more model dependent than BB derived constraints on r.

Figure 8 compares signal levels and current noise uncertainties in the critical $\ell \sim 80$ band power (updated from Fig. 13 of BKP [16]). A second season of 95 GHz Keck Array data has already been recorded (in 2015) and will push the 95 × 95 point down by a factor of 2. During 2015 two receivers were also operated in a third band centered on 220 GHz, producing deep maps that will improve dust separation. These 2015 data are under analysis and will be reported on in a future paper. In addition, BICEP3 began operations in 2015 in the 95 GHz band.

In this Letter, we have presented an analysis of all BICEP2/Keck data up through the 2014 season, adding, for the first time, 95 GHz data from the Keck Array. We have updated our multifrequency likelihood analysis with a more extensive foreground parametrization and the inclusion of external data from the 23 and 33 GHz bands of WMAP, in addition to all seven polarized bands of Planck. The baseline analysis yields $r_{0.05} = 0.028^{+0.026}_{-0.025}$

and $r_{0.05} < 0.09$ at 95% confidence, constraints that are robust to the variations explored in analysis and priors. With this result, B modes now offer the most powerful limits on inflationary gravitational waves, surpassing constraints from temperature anisotropies and other evidence for the first time. With upcoming multifrequency data, the B-mode constraints can be expected to steadily improve.

A COSMOMC module containing the BICEP2/Keck data as used in this Letter is available by following the link in Ref. [31].

The Keck Array project has been made possible through support from the National Science Foundation under Grants No. ANT-1145172 (Harvard), No. ANT-1145143 (Minnesota), and No. ANT-1145248 (Stanford), and from the Keck Foundation (Caltech). The development of antenna-coupled detector technology was supported by the JPL Research and Technology Development Fund and Grants No. 06-ARPA206-0040 and No. 10-SAT10-0017 from the NASA APRA and SAT programs. The development and testing of focal planes were supported by the Gordon and Betty Moore Foundation at Caltech. Readout electronics were supported by a Canada Foundation for Innovation grant to UBC. The computations in this Letter were run on the Odyssey cluster supported by the FAS Science Division Research Computing Group at Harvard University. The analysis effort at Stanford and SLAC is partially supported by the U.S. DOE Office of Science. We thank the staff of the U.S. Antarctic Program and, in particular, the South Pole Station without whose help this research would not have been possible. Most special thanks go to Robert Schwarz and Steffen Richter. We thank all those who have contributed past efforts to the BICEP-Keck Array series of experiments, including the BICEP1 team. We also thank the Planck and WMAP teams for the use of their data.

*jmkovac@cfa.harvard.edu
†pryke@physics.umn.edu

[1] A. A. Penzias and R. W. Wilson, A measurement of excess antenna temperature at 4080 Mc/s, Astrophys. J. **142**, 419 (1965).
[2] P. A. R. Ade *et al.* (Planck Collaboration), Planck 2015 results. XIII. Cosmological parameters, arXiv:1502.01589.
[3] M. Kamionkowski and E. D. Kovetz, The quest for B modes from inflationary gravitational waves, arXiv:1510.06042.
[4] A. H. Guth, D. I. Kaiser, and Y. Nomura, Inflationary paradigm after Planck 2013, Phys. Lett. B **733**, 112 (2014).
[5] A. Ijjas, P. J. Steinhardt, and A. Loeb, Inflationary schism, Phys. Lett. B **736**, 142 (2014).
[6] J. M. Kovac, E. M. Leitch, C. Pryke, J. E. Carlstrom, N. W. Halverson, and W. L. Holzapfel, Detection of polarization in the cosmic microwave background using DASI, Nature (London) **420**, 772 (2002).
[7] P. A. R. Ade *et al.* (POLARBEAR Collaboration), A measurement of the cosmic microwave background B-mode polarization power spectrum at sub-degree scales with POLARBEAR, Astrophys. J. **794**, 171 (2014).
[8] R. Keisler *et al.*, Measurements of sub-degree B-mode polarization in the cosmic microwave background from 100 square degrees of SPTpol data, arXiv:1503.02315.
[9] D. Barkats *et al.* (BICEP1 Collaboration), Degree-scale cosmic microwave background polarization measurements from three years of BICEP1 data, Astrophys. J. **783**, 67 (2014).
[10] P. A. R. Ade *et al.* (BICEP2 Collaboration), Detection of B-Mode Polarization at Degree Angular Scales by BICEP2, Phys. Rev. Lett. **112**, 241101 (2014).
[11] P. A. R. Ade *et al.* (BICEP2 and Keck Array Collaborations), BICEP2/Keck array V: Measurements of B-mode polarization at degree angular scales and 150 GHz by the Keck array, Astrophys. J. **811**, 126 (2015).
[12] P. A. R. Ade *et al.* (Planck Collaboration), Planck intermediate results. XIX. An overview of the polarized thermal emission from Galactic dust, Astron. Astrophys. **576**, A104 (2015).
[13] R Adam *et al.* (Planck Collaboration), Planck intermediate results. XXX. The angular power spectrum of polarized dust emission at intermediate and high Galactic latitudes, arXiv:1409.5738 [Astron. Astrophys. (to be published)].
[14] R. Flauger, J. C. Hill, and D. N. Spergel, Toward an understanding of foreground emission in the BICEP2 region, J. Cosmol. Astropart. Phys. 08 (2014) 039.
[15] M. J. Mortonson and U. Seljak, A joint analysis of Planck and BICEP2 B modes including dust polarization uncertainty, J. Cosmol. Astropart. Phys. 10 (2014) 035.
[16] P. A. R. Ade *et al.* (BICEP2/Keck and Planck Collaborations), Joint Analysis of BICEP2/Keck Array and Planck Data, Phys. Rev. Lett. **114**, 101301 (2015).
[17] P. A. R. Ade *et al.* (BICEP2 Collaboration), BICEP2. II. Experiment and three-year data set, Astrophys. J. **792**, 62 (2014).
[18] P. A. R. Ade *et al.* (BICEP2, Keck Array, and Spider Collaborations), Antenna-coupled TES bolometers used in BICEP2, Keck array, and spider, Astrophys. J. **812**, 176 (2015).
[19] See Supplemental Material at http://link.aps.org/supplemental/10.1103/PhysRevLett.116.031302, which includes Refs. [20,21], for appendixes.
[20] S. K. Choi and L. A. Page, Polarized galactic synchrotron and dust emission and their correlation, arXiv:1509.05934.
[21] J. Dunkley *et al.*, Prospects for polarized foreground removal, AIP Conf. Proc. **1141**, 222 (2009).
[22] See http://www.cosmos.esa.int/web/planck/pla.
[23] R. Adam *et al.* (Planck Collaboration), Planck 2015 results. I. Overview of products and scientific results, arXiv:1502.01582.
[24] See http://lambda.gsfc.nasa.gov/product/map/dr5/m_products.cfm.
[25] C. L. Bennett *et al.*, Nine-year Wilkinson microwave anisotropy probe (WMAP) observations: Final maps and results, Astrophys. J. Suppl. Ser. **208**, 20 (2013).
[26] P. A. R. Ade *et al.* (Planck Collaboration), Planck 2015 results. XII. Full focal plane simulations, arXiv:1509.06348.

[27] S. Hamimeche and A. Lewis, Likelihood analysis of CMB temperature and polarization power spectra, Phys. Rev. D **77**, 103013 (2008).

[28] A. Lewis and S. Bridle, Cosmological parameters from CMB and other data: A Monte Carlo approach, Phys. Rev. D **66**, 103511 (2002).

[29] P. A. R. *et al.* (Planck Collaboration), Planck intermediate results. XXII. Frequency dependence of thermal emission from Galactic dust in intensity and polarization, Astron. Astrophys. **576**, A107 (2015).

[30] U. Fuskeland, I. K. Wehus, H. K. Eriksen, and S. K. Næss, Spatial variations in the spectral index of polarized synchrotron emission in the 9 yr WMAP sky maps, Astrophys. J. **790**, 104 (2014).

[31] See http://bicepkeck.org.